Available online at www.sciencedirect.com
SCIENCE DIRECT®
Precambrian Research 122 (2003) 235–251
Precambrian Research
www.elsevier.com/locate/precamres

Low-pressure metamorphism and leucogranite magmatism, northeastern Yeongnam Massif, Korea: implication for Paleoproterozoic crustal evolution

Jeongmin Kim [a,b], Moonsup Cho [b,*]

[a] *Korea Basic Science Institute, Taejon 305-333, South Korea*
[b] *School of Earth and Environmental Sciences, Seoul National University, Seoul 151-742, South Korea*

Received 19 December 2001; received in revised form 22 April 2002; accepted 22 April 2002

Abstract

The northeastern Yeongnam Massif consists primarily of pelitic to psammopelitic metasedimentary rocks, together with garnet-bearing leucogranites and granitic gneisses. Metapelitic mineral assemblages define three progressive metamorphic zones of the low-pressure facies series: cordierite, sillimanite, and garnet zones with increasing temperature. Metamorphic grade ranges from lower-amphibolite to lower-granulite facies, reaching 750–800 °C and 4–6 kbar in migmatitic gneisses. Geochemical characteristics, such as the enrichments of Rb and Ba relative to Sr, high K contents, and negative $\varepsilon_{Nd\,(1.9\,Ga)}$ values, indicate that peraluminous leucogranites were produced primarily by the fluid-absent melting of supracrustal rocks. Trace element characteristics of leucogranites are generally compatible with those of volcanic arc granites, and the widespread crustal melting may be attributed largely to magmatic heat flux in an arc environment. Whole rock Pb–Pb ages suggest that leucogranite intruded at ca. 1.93–1.86 Ga into the granitic gneiss, formed by an earlier magmatic episode at ca. 1.95 Ga. These ages are compatible with those of felsic magmatism reported from other parts of the Yeongnam Massif. Our results, in conjunction with the available geochronologic data, suggest that four stages of Precambrian crustal evolution are represented in the Yeongnam Massif: (1) the formation of proto-crust at ca. 2.9–2.5 Ga, and felsic magmatic episodes primarily at (2) ca. 2.1 Ga, (3) 1.95 Ga, and (4) 1.9 Ga. In particular, the last tectonothermal event produced widespread low-pressure type metamorphism in association with the emplacement of leucogranite, and is correlative with the Luliangian Orogeny in North China.

Keywords: Yeongnam Massif; LP/HT metamorphism; Leucogranite; Paleoproterozoic; Pb–Pb and Sm–Nd ages

1. Introduction

The Korean Peninsula, situated at the eastern margin of the Eurasian continent, primarily consists of two Phanerozoic mobile belts; the Imjingang belt and the Ogcheon fold belt, and three Precambrian basement terrains; the Nangrim, Gyeonggi and Yeongnam Massifs from north to south (Fig. 1). Tectonic evolution of the two mobile belts has been the focus of recent investigations (Cluzel, 1992; Cho et al., 1995; Ree et al., 1996, 2001), because they may correspond to an eastward extension of the continental collision belt between the North China Block and the South China Block.

The North China Block and South China Block are two major cratons in East Asia, being separate until the Late Paleozoic (e.g., Yin and Nie, 1993; Zhao

* Corresponding author. Fax: +82-2-871-3269.
E-mail address: moonsup@snu.ac.kr (M. Cho).

0301-9268/02/$ – see front matter
PII: S0301-9268(02)00213-9

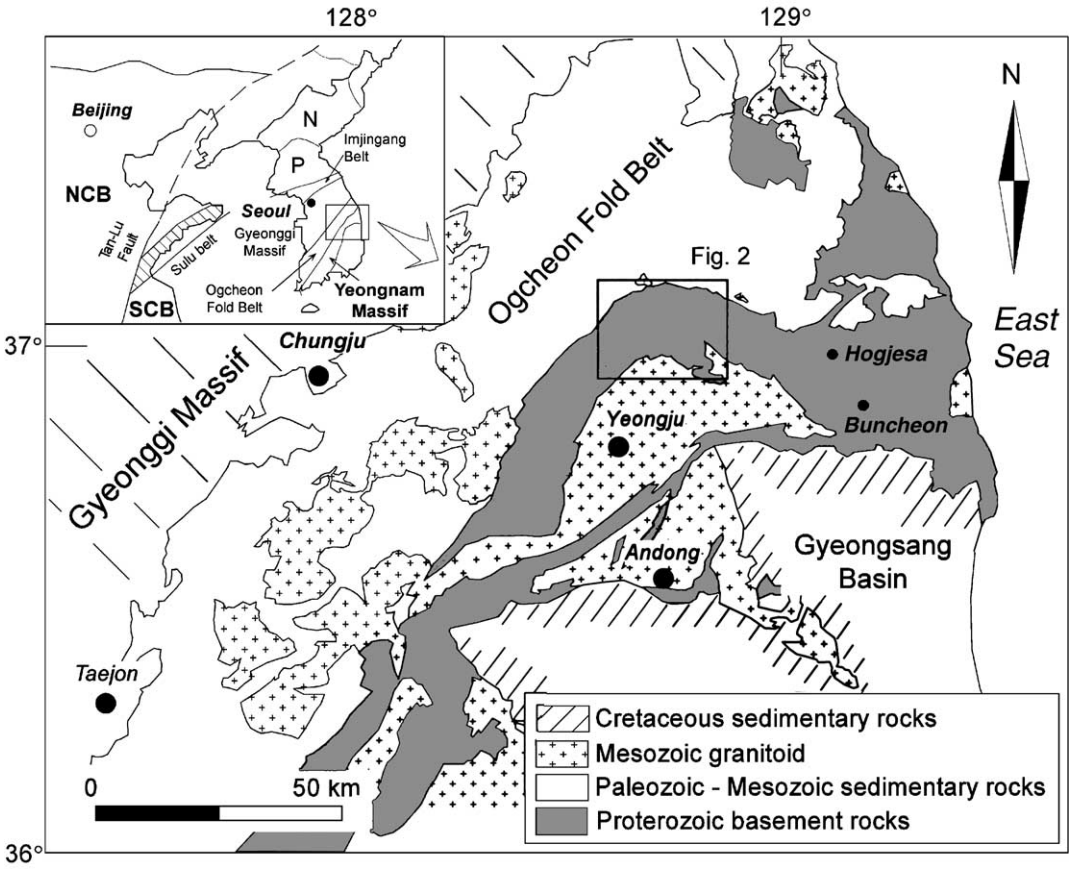

Fig. 1. Simplified geologic map of the northern Yeongnam Massif (after KIGAM, 1995) showing the location of the study area. Inset: location of the study area. N: Nangrim Massif, P: Pyeongnam Basin, NCB: North China Block, SCB: South China Block.

et al., 1996). During the Late Permian to Early Triassic, the two Chinese blocks were assembled along the Qinling-Dabie-Sulu belt, characterized by the occurrence of ultrahigh-pressure metamorphic rocks. The indentation model of Yin and Nie (1993) and the crustal detachment model of Li (1994), accounting for not only the large-scale tectonics but also sedimentary records in the Korean Peninsula, have invoked an on-going controversy on the presence of the suture zone in Korea (Cho et al., 1995; Ree et al., 1996; Chough et al., 2000; Cheong et al., 2000; Cho, 2001). For example, according to Yin and Nie's (1993) model, the Yeongnam Massif and Gyeonggi Massif were separate blocks correlative with the North China Block and South China Block, respectively. However, the lack of direct evidence for continental collision, e.g., ophiolites or (ultra) high-pressure metamorphic rocks, prevents us from establishing unequivocal relationships between the Precambrian massifs in Korea and the cratonic blocks in China.

A fuller understanding of crustal evolution for the basement rocks in Korea could be beneficial not only for the delineation of Permo-Triassic continental collisional processes but also for the reconstruction of the Proterozoic supercontinent in East Asia (Li, 1998; Zhao, 2001). Recently, Lee et al. (2000) suggested on the basis of metamorphic, geochronologic and isotopic studies that the basement rocks in the central Gyeonggi Massif have experienced Archean-Paleoproterozoic crustal growth, ca. 1.87 Ga granulite-facies metamorphism, and Permian-Triassic reactivation. Such high-grade metamorphic terrains

are widespread in the Yeongnam Massif, but relatively few petrologic studies have been undertaken (e.g., Kim and Cho, 1994; Cheong et al., 2000). Thus, many uncertainties remain with regard to the P-T-t evolution, including the relationship between regional metamorphism and granitic magmatism. In addition, the crustal growth history and tectonic framework of the Yeongnam Massif are poorly constrained.

In this article, we report mineral parageneses and P–T conditions of low-pressure/high-temperature (LP/HT) metasedimentary rocks in the northeastern Yeongnam Massif. The occurrence of prograde successions of medium-grade schists is unique to the northeastern part of the Yeongnam Massif, because the rest is predominated by upper amphibolite to granulite facies gneisses. We also report geochemical characteristics and petrogeneses of garnet-bearing leucogranites commonly associated with the metasedimentary rocks. Moreover, Sm–Nd and Pb–Pb isotopic systematics were used to unravel the temporal relationship between granitic magmatism and high-grade metamorphism. Finally, we discuss the Paleoproterozoic crustal evolution of the Yeongnam Massif, in the context of the Precambrian tectonics of East Asia.

2. Geological setting

The Yeongnam Massif is a polymetamorphic terrain bounded to the north by the Ogcheon fold belt, and overlain by thick Cretaceous sedimentary-volcanic sequences to the southeast. This massif consists primarily of high-grade gneisses such as quartzo-feldspathic banded gneiss, migmatitic gneiss, porphyroblastic gneiss, and granitic gneiss, together with minor biotite schist and metapelitic schist. Amphibolites and calc-silicate rocks also occur in subordinate amounts. Metamorphic grade of the Yeongnam Massif ranges from amphibolite to granulite facies.

The study area, situated in the northeastern part of the Yeongnam Massif, mainly comprises two lithologic units; metasedimentary rocks and granitic rocks such as leucogranite and granitic gneiss (Fig. 2). The former was previously known as the Yulri Group (Reedman and Um, 1975) or the Taebaeksan schist complex (Lee and Kim, 1984). To the north, Paleozoic shallow marine sedimentary sequences (the Joseon Supergroup) unconformably overlie the Precambrian basement rocks. To the south, the Late Triassic Yeongju granite intrudes into the Precambrian gneisses, leading to the formation of minor thermal aureoles. Its emplacement pressure was estimated from aluminum-in-hornblende geobarometry as ca. 6 kbar (Hong, 2001).

Metasedimentary rocks consist of interbedded pelitic and psammopelitic schists, showing penetrative foliations subparallel to lithologic layers and dipping generally to the north. Metamorphic grade increases southward from lower amphibolite to lower granulite facies over a distance of ca. 10–15 km. Three metamorphic zones are defined on the basis of mineral assemblages (Fig. 2); these are, from north to south, the cordierite, sillimanite, and garnet zones. This progression of metamorphic zones conforms to that of a LP/HT metamorphic terrain (e.g., Morand, 1990; Miyashiro, 1994). In high-temperature zones above the sillimanite-in isograd, pelitic rocks are variably migmatized to form metatexite to diatexite. Diatexitic migmatites show petrographic characteristics similar to those of leucogranites, except for widespread occurrences of schlieren and xenolith in the former. The boundary between diatexitic migmatite and leucogranite is transitional.

Garnet-bearing leucogranites intrude as small-scale stocks, sills and subconcordant dykes into pelitic to psammopelitic schists and granitic gneisses. Leucogranites occur even in the cordierite zone, and show no deformational fabric. An extensive network of pegmatite dykes, up to several meters wide, often develops in association with leucogranites. These pegmatites are undeformed and contain gray K-feldspar, which is characteristic of the Precambrian granitoids in the Yeongnam Massif, including the Hongjesa granitic batholith (Fig. 1; Kim and Cho, 1994). Granitic gneisses occur as small-scale stocks intruding metasedimentary rocks, and their foliation is generally parallel to that of the country rocks. The preservation of euhedral plagioclase megacrysts suggests an igneous origin for the granitic gneiss. Metamorphic minerals such as garnet, cordierite and/or sillimanite commonly occur in granitic gneiss. Both leucogranite and granitic gneiss often contain abundant xenoliths of metasedimentary rocks.

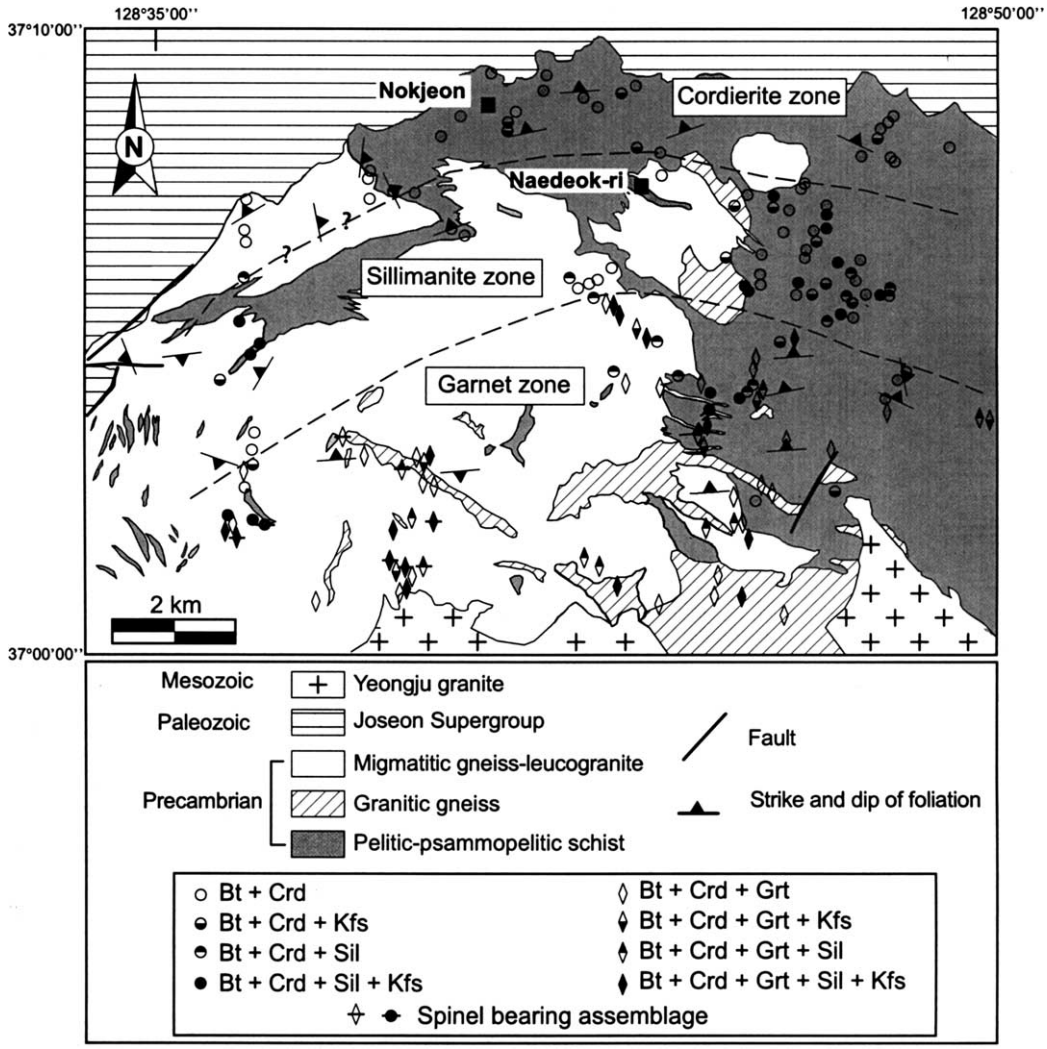

Fig. 2. Schematic geologic map of the study area adopted from Lee and Kim (1965) and Lee (1966). Mineral assemblages are also shown for representative samples from each metamorphic zone. Mineral abbreviations are from Kretz (1983).

3. Petrography

3.1. Peltic to psammopelitic schists

Various mineral assemblages of pelitic-psammopelitic schists (Fig. 2) are characterized by the occurrence of cordierite, sillimanite, and garnet together with quartz, plagioclase, and K-feldspar. The preferred orientation of biotite and fibrolitic sillimanite defines the penetrative foliation. Cordierite occurs as ubiquitous porphyroblasts ranging up to 2 cm in size, and commonly contains numerous inclusions of quartz, biotite, and aggregates of fibrous or prismatic sillimanite. These inclusions are commonly oriented subparallel to the external foliation. Fibrolite predominates in the sillimanite zone, whereas prismatic sillimanite occurs in the garnet zone. Texturally late poikiloblasts of andalusite occur in the garnet zone, and together with fine-grained biotite, often replace garnet and cordierite. Oligoclase ($An_{12–25}$) and microcline occur as euhedral to subhedral grains. Plagioclase is common in psammopelitic schists, but uncommon

or rare in metapelitic schists. Some porphyroblasts of microcline locally preserve inclusion trails of biotite oblique to the external foliation. Most grains of muscovite and chlorite occur as retrograde phases. Accessory minerals in pelitic to psammitic gneisses include ilmenite, apatite, zircon and tourmaline.

3.2. Migmatitic gneisess

Stromatic migmatitic gneiss first appears in the sillimanite zone. Patchy or vein-type leucosomes are 3–20 mm wide and occur as bedding-parallel layers or boudins in low strain zones. Psammopelitic schists, in contrast to pelitic ones, commonly contain minor amounts of leucosome, reflecting a bulk compositional control on the amount of melt produced and frozen in-situ. Mineral assemblages of leucosome primarily consist of quartz, oligoclase and microcline, together with minor amounts of secondary muscovite and chlorite.

Metatexitic migmatites are widespread in the garnet zone, and their leucosomes contain garnet and/or cordierite. Melanosomes consist primarily of medium- to coarse-grained biotite, sillimanite, cordierite, garnet, quartz, spinel and ilmenite. Large garnet porphyroblasts (10–20 mm in diameter), containing inclusions of quartz, biotite, sillimanite, cordierite and ilmenite, occur at the interface between leucosome and melanosome. These mineral inclusions define internal foliation subparallel to external one, similar to textural relationship found in cordierite porphyroblasts. This observation is corroborated by post-tectonic growth of cordierite and garnet porphyroblasts that apparently grow overprinting the penetrative foliation.

Fine-grained ilmenite develops along the margin of biotite in melanosomes, reflecting the instability of biotite during incongruent melting (Brown, 1983). Deep-green hercynitic spinel commonly occurs in quartz-absent domains as fine-grained equidimensional inclusions within garnet, sillimanite and cordierite.

Diatexitic migmatites prevail in local domains adjacent to the leucogranite. Quartzofeldspathic diatexites are commonly entrained with biotite-rich schlieren containing poly-mineralic aggregates of garnet, cordierite, biotite and sillimanite. The mineral assemblage and the absence of melt-derived textures such as idioblastic crystal faces and graphic intergrowths (Ashworth and McLellan, 1985; Vernon and Collins, 1988) indicate the restitic origin of the schlieren.

3.3. Granitic rocks

Leucogranites are medium to coarse-grained, and contain small amounts of biotite, muscovite and garnet, together with abundant quartz, plagioclase and K-feldspar. Garnet is ubiquitous and occurs as equigranular euhedral grains containing few mineral inclusions. The crystal habit and high spessartine content ($Alm_{77}Sps_{14}Prp_8Grs_1$), in the absence of other ferromagnesian minerals in leucogranites, favor a magmatic origin for the garnet. This inference is corroborated by the occurrence of garnet-bearing leucogranites even in the cordierite zone. In addition, the compositional difference of garnet between leucogranite and high-grade gneiss precludes the possibility of xenocrystic origin. Proportions of K-feldspar to plagioclase are variable, and K-feldspar megacrysts up to 15 cm long occur in pegmatitic leucogranites. Muscovite commonly shows poikilitic texture indicating late-stage crystallization. Sillimanite occurs as either fine-grained euhedral prisms or interstitial fibrolitic mats in the mica-rich schlieren. Tourmaline occurs as an accessory phase.

Granitic gneisses are medium to coarse-grained, and consist primarily of quartz, plagioclase, K-feldspar and biotite, together with minor amounts of cordierite and garnet. Garnet occurs as inclusion-rich anhedral crystals and commonly shows embayed grain boundaries. The common occurrence of biotite inclusions suggests that garnet was formed by a biotite-consuming reaction. Minor sillimanite grains are present in some granitic gneisses. Mineral assemblages of granitic gneiss are indicative of high-grade metamorphic conditions, compatible with that of the adjacent metasedimentary rocks. Zircon, tourmaline and ilmenite occur as accessory phases.

4. Metamorphic conditions

Progressive mineral assemblages (+ quartz + oligoclase±K-feldspar) develop in metapelitic schists: biotite + cordierite; biotite + cordierite + sillimanite; biotite + cordierite + garnet; and biotite + cordierite + garnet + sillimanite (Fig. 2). Such variations are the product of prograde metamorphic reactions, and can be accounted for by utilizing a simple model system, K_2O–FeO–MgO–Al_2O_3–SiO_2–H_2O (KFMASH). We

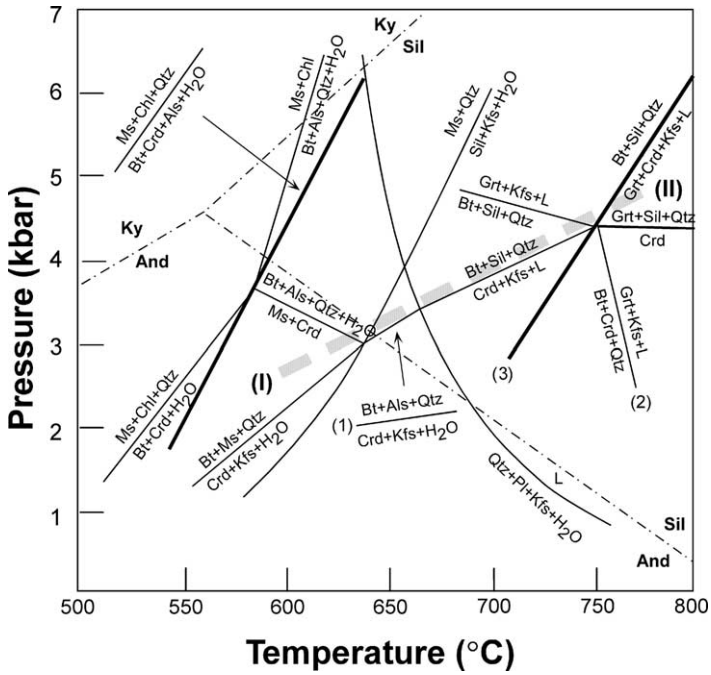

Fig. 3. Simplified petrogenetic grid of metapelites in the KFMASH system (after Pattison, 1991). Univariant reactions represent the isopleths of constant Fe/(Fe + Mg) values of 0.55 in cordierite. Heavy dashed line indicates the approximate metamorphic field gradient. I and II represent the P–T conditions for the cordierite and garnet zones, respectively.

adopted the petrogenetic grid of Pattison (1991) constructed at constant X_{Fe} (=Fe/(Fe + Mg)) of 0.55 in cordierite (Kim and Cho, unpublished data; Fig. 3).

The ubiquitous occurrence of cordierite porphyroblasts containing inclusions of biotite and sillimanite suggests that the following continuous reaction was operative in the sillimanite zone:

biotite + sillimanite + quartz

→ cordierite + K-feldspar + H_2O. (1)

The inclusions of sillimanite, biotite, cordierite and quartz in garnet, and the dissolution texture of cordierite in the garnet zone suggest that the garnet-forming reaction was governed by:

biotite + cordierite + quartz

→ garnet + K-feldspar + H_2O (or liquid). (2)

The occurrence of euhedral cordierite and garnet at the interface between leucosome and melanosome and the ubiquity of biotite+sillimanite in the mesosome of migmatitic gneiss indicate that garnet and/or cordierite grew as a peritectic phase during the melting stage through the reaction:

biotite + sillimanite + quartz

→ garnet + cordierite + K-feldspar + liquid. (3)

Hercynitic spinel occurs only as inclusions in sillimanite, garnet and cordierite. The spinel-forming reaction (e.g., biotite+sillimanite → cordierite+spinel+K-feldspar+melt, Pattison and Harte, 1991) occurs at higher temperature than the garnet-forming reaction in the model system. However, the high gahnite content can stabilize spinel at lower temperatures. The removal of melt also facilitates the formation of spinel in the biotite + cordierite + sillimanite + quartz assemblage (Whittington et al., 1998). Therefore, the occurrence of spinel does not necessarily imply a significant difference in metamorphic temperatures to the garnet zone.

The stable coexistence of biotite and cordierite without primary chlorite and the absence of sillimanite

or in situ melting in the cordierite zone indicate that the peak metamorphic temperature was higher than ca. 530 °C at 2 kbar but less than ca. 640 °C (region I in Fig. 3). Peak metamorphic conditions of migmatitic gneisses reached 750–800 °C and 4–6 kbar (region II in Fig. 3), where the mineral assemblage of biotite + sillimanite + cordierite + garnet + K-feldspar is stable. This result is corroborated by average pressure and temperature in the garnet zone (705–765 °C and 4.5–6.2 kbar; Kim and Cho, unpublished data), estimated using the computer program TWQ 2.02 and its thermodynamic dataset (Berman, 1991; Aranovich and Berman, 1997). Fig. 4 shows an example of our calculation for a garnet-zone sample, using the K_2O–CaO–FeO–MgO–Al_2O_3–SiO_2–H_2O (KCFMASH) system.

The prograde mineral assemblages and estimated P–T conditions are compatible with those of the low-pressure facies series (Miyashiro, 1961). Furthermore, the occurrence of the high-temperature assemblage biotite–garnet–sillimanite–K-feldspar–cordierite, the prevalence of cordierite in medium-grade schists, and the absence of staurolite and kyanite are accounted for by the facies series of type 2a of Pattison and Tracy (1991).

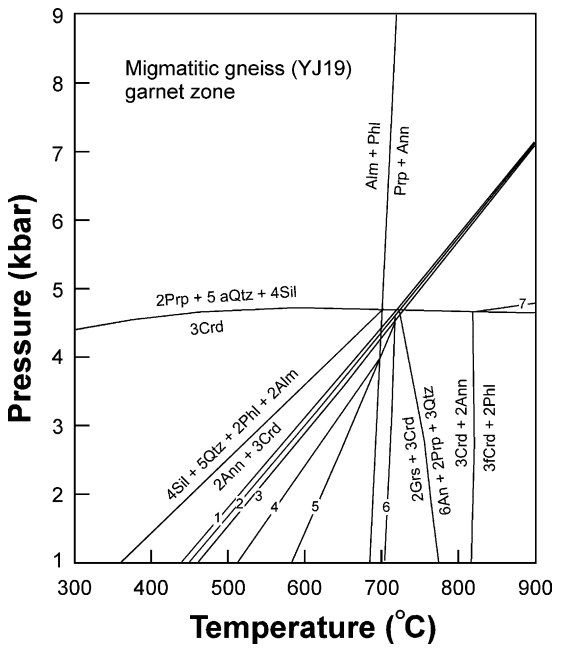

Fig. 4. TWQ results in the KCFMASH system for a garnet-zone sample (YJ19). Reactions: (1) 2Alm + 5Qtz + 4Sil = 3fCrd; (2) Grs + Qtz + 2Sil = 3An; (3) 6Sil + 5Grs + 3fCrd = 2Alm + 15An; (4) 6Sil + 5Grs + 3Crd + 2Ann = 2Alm + 15An + 2Phl; (5) 3Crd+2Alm = 3fCrd+2Ann; (6) 3Crd+2Alm = 3fCrd+2Prp; (7) 2Ann + 2Prp + 5Qtz + 4Sil = 2Phl + 3fCrd. Mineral abbreviations are from Kretz (1983).

5. Geochemistry of leucogranites

5.1. Analytical techniques

Eleven samples of medium- to coarse-grained, garnet-bearing leucogranites were crushed and ground in a tungsten carbide ball mill. Major element data were obtained using a Shimadzu X-ray fluorescence spectrometer at Seoul National University. Trace elements and rare earth elements (REE) were measured using the inductively-coupled plasma mass spectrometer and atomic emission spectrometer at Korea Basic Science Institute.

Isotopic analyses for Sm–Nd and Pb were carried out on a VG54-30 thermal ionization mass spectrometer in dynamic and static multicollector modes, respectively. The details of the experimental procedure are available in Cheong et al. (2000). Nd isotopic compositions were normalized to $^{146}Nd/^{144}Nd = 0.7219$. The $^{143}Nd/^{144}Nd$ ratios were corrected to the La Jolla standard ($^{143}Nd/^{144}Nd = 0.511839 \pm 0.000007$, 2σ, $n = 8$). The Pb isotopic ratios were corrected for instrumental fractionation using average values of the NBS 981 standard. External precision for $^{143}Nd/^{144}Nd$ ratios is 0.004%, and $^{147}Sm/^{144}Nd$ ratios are reproducible to 0.5%. The ε_{Nd} values were calculated on the basis of an $^{147}Sm/^{144}Nd$ value of 0.1967 for chondrite-normalized uniform reservoir (CHUR) and a present-day $^{143}Nd/^{144}Nd$ value of 0.512638 (Jacobsen and Wasserburg, 1980). For age calculations, isotopic data were regressed after York (1969) and Ludwig (1992). Uncertainties in ages are reported at the 95% confidence level. Depleted-mantle model ages (T_{DM}) were calculated following Nägler and Kramers (1998).

5.2. Major elements

The SiO_2 contents of leucogranite show a narrow range of 69−74 wt.%, and the K_2O contents apparently decrease with increasing Na_2O (Table 1). High A/CNK (=Al_2O_3/(CaO + Na_2O + K_2O)) values of

Table 1
Major, trace and rare earth element data for the leucogranite

	Sample										
	K47-1	K54	JJ22-1	NJ11	YJ02	YJ03	YJ08	YJ13	YJ21	YP28-2	YP28-3
Major element concentration (wt.%)											
SiO_2	72.95	72.72	71.89	72.78	72.68	73.71	72.74	74.02	68.55	73.86	72.10
Al_2O_3	14.66	14.75	14.37	14.52	14.55	14.53	14.75	14.56	16.23	14.93	14.34
Fe_2O_3	1.02	0.79	0.63	0.71	0.86	1.34	1.35	0.82	3.93	0.56	1.13
TiO_2	0.12	0.03	0.04	0.03	0.02	0.02	0.12	0.01	0.01	0.03	0.01
MnO	0.02	0.07	0.02	0.08	0.06	0.19	0.05	0.09	0.64	0.03	0.16
CaO	1.52	0.64	0.97	1.03	0.52	0.47	1.31	0.62	1.11	1.19	0.41
MgO	0.29	0.20	0.24	0.06	0.15	0.18	0.33	0.12	0.20	0.09	0.10
K_2O	4.94	5.91	4.41	4.86	5.78	4.69	3.11	4.82	3.93	2.70	6.97
Na_2O	3.51	3.48	3.94	4.15	3.62	3.80	4.39	3.84	3.98	5.27	3.11
P_2O_5	0.21	0.11	0.29	0.12	0.16	0.19	0.18	0.36	0.29	0.14	0.42
LOI	0.48	0.49	0.81	0.75	0.66	0.89	0.75	0.49	0.91	0.40	0.45
Total	99.72	99.19	97.61	99.09	99.06	100.01	99.08	99.75	99.78	99.20	99.20
A/CNK	1.057	1.112	1.105	1.041	1.107	1.194	1.139	1.151	1.268	1.087	1.071
Normative concentration											
Q	30.61	28.76	30.61	28.47	29.04	33.16	32.99	33.02	27.86	30.91	26.43
C	1.16	1.69	2.03	0.80	1.78	2.80	2.14	2.82	4.02	1.49	2.10
Z	0.02	0.00	0.00	0.02	0.01	0.01	0.02	0.00	0.00	0.00	0.00
Or	29.47	35.40	27.25	29.25	34.77	28.02	18.77	28.78	23.77	16.18	42.72
Ab	29.93	29.81	34.78	35.71	31.13	32.44	37.82	32.74	34.38	45.13	27.22
An	6.58	2.67	3.30	4.57	1.58	1.14	5.65	0.59	4.15	5.11	0.00
Hy	0.73	0.50	0.62	0.15	0.38	0.45	0.84	0.30	0.51	0.23	0.26
Mt	0.00	0.14	0.00	0.17	0.14	0.52	0.13	0.29	2.13	0.00	0.54
Cm	0.00	0.00	0.00	0.00	0.00	0.00	0.00	0.00	0.00	0.00	0.00
Hm	1.03	0.78	0.66	0.60	0.78	0.99	1.29	0.62	2.54	0.57	0.80
Il	0.03	0.06	0.06	0.06	0.04	0.04	0.00	0.02	0.01	0.05	0.02
Ru	0.11	0.00	0.01	0.00	0.00	0.00	0.00	0.00	0.00	0.01	0.00
Ap	0.52	0.27	0.72	0.29	0.39	0.46	0.44	0.86	0.71	0.34	1.06
Pr	0.02	0.01	0.00	0.01	0.01	0.03	0.02	0.00	0.00	0.02	0.00
Spod	0.06	0.01	0.00	0.02	0.02	0.04	0.12	0.00	0.00	0.06	0.00
Total	100.24	100.11	100.06	100.12	100.06	100.09	100.23	100.05	100.08	100.1	101.13
Trace element concentration (ppm)											
Rb	116.72	99.06	140.21	115.01	142.26	130.24	126.03	172.52	127.96	82.56	238.73
Sr	191.88	152.32	78.77	139.97	36.89	50.59	200.12	32.42	105.00	117.06	96.08
Ba	1116.44	506.55	90.89	435.15	28.74	92.70	599.94	0.47	259.16	79.40	184.18
Y	7.61	11.74	10.20	4.53	6.29	5.37	22.57	7.50	10.71	5.92	5.63
Nb	2.69	0.81	4.07	2.93	1.01	2.36	0.30	0.22	10.58	0.17	0.74
Ta	0.61	0.40	1.84	0.92	0.60	1.94	1.51	0.39	2.15	0.29	2.04
Rare earth element concentration (ppm)											
La	23.81	4.19	4.40	10.50	1.36	2.83	4.80	1.55	9.50	2.75	1.05
Ce	46.52	6.92	9.03	20.29	2.26	4.60	8.76	3.12	19.19	4.80	1.47
Pr	5.56	0.76	1.05	2.27	0.22	0.53	0.99	0.35	2.21	0.50	0.13
Nd	18.44	2.43	3.79	7.28	0.60	1.49	3.38	1.18	7.28	1.59	0.40
Sm	3.51	0.56	1.19	1.68	0.18	0.42	0.91	0.41	2.13	0.45	0.10
Eu	1.07	0.67	0.35	0.61	0.06	0.10	0.89	0.10	0.53	0.30	0.34
Gd	3.44	0.64	1.39	1.75	0.22	0.44	1.16	0.43	1.99	0.62	0.16
Tb	0.40	0.10	0.30	0.29	0.06	0.11	0.22	0.11	0.48	0.15	0.06
Dy	1.76	0.97	1.84	1.89	0.53	0.84	1.53	0.86	3.40	0.99	0.69
Ho	0.23	0.25	0.33	0.36	0.11	0.16	0.31	0.16	0.73	0.16	0.19
Er	0.56	0.98	0.87	1.16	0.39	0.52	0.93	0.54	2.71	0.49	0.80
Tm	0.08	0.19	0.13	0.19	0.09	0.12	0.15	0.12	0.59	0.08	0.18
Yb	0.52	1.67	0.77	1.51	0.85	0.99	1.09	0.93	5.35	0.57	1.57
Lu	0.07	0.27	0.10	0.21	0.13	0.13	0.17	0.14	0.85	0.07	0.26
La_N/Lu_N	4.27	4.73	2.33	3.94	4.73	4.20	3.32	2.36	2.81	3.85	6.38
Eu/Eu*	0.98	3.56	0.83	1.12	1.01	0.72	2.72	0.69	0.79	1.80	8.03

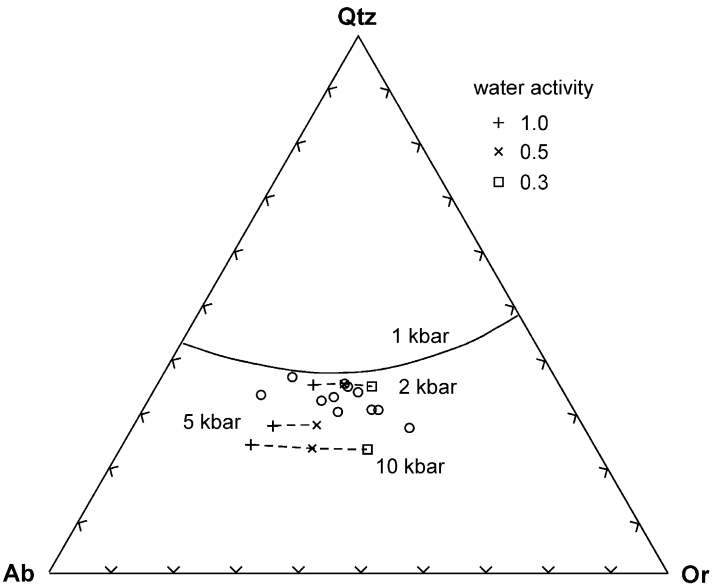

Fig. 5. Normative Qtz–Or–Ab compositions of leucogranite (○). Also shown are thermal minimum and ternary eutectic compositions determined at various H_2O pressures and activities in haplogranitic systems (Holtz et al., 1992; Ebadi and Johannes, 1991).

1.04−1.27 together with normative corundum reflect the peraluminous nature of the leucogranite. The leucogranite shows no systematic trend in the normative quartz–orthoclase–albite (Qtz–Or–Ab) diagram (Fig. 5). However, significant variations in the Or/Ab ratios at constant Qtz content are apparent in Fig. 5, and may result from change in the activity of H_2O during granitic melt formation (Ebadi and Johannes, 1991; Holtz et al., 2001). Samples with higher Or component than that of the thermal minimum may be attributed to fluid-absent melting of micas which will generate potassic magma and restitic K-feldspar (Inger and Harris, 1993). The emplacement pressure is approximately estimated from Fig. 5 to be 2−5 kbar, compatible with metamorphic pressures inferred from the metasedimentary rocks. Although high anorthite components in plagioclase may affect the minimum melt composition in the granite system (Johannes and Holtz, 1996), the CaO content in leucogranites is insignificant.

5.3. Rare earth and trace elements

Leucogranites have low total REE abundances (7–57 ppm, except for one sample K47-1 with 105 ppm; Table 1), and show concave-upward chondrite-normalized patterns with variable LREE enrichment ($La_N/Lu_N = 2.3–6.4$; Fig. 6). Accumulation of magmatic garnet may account for the HREE enrichment. Low total REE abundances of leucogranite may result from significant progression of fractional crystallization, or small degree of partial melting, or REE-depleted composition of the source rock (e.g., Nabelek and Glascock, 1995). However, the second explanation is incompatible with the widespread occurrence of leucogranite, whereas the last one is in contrast to high REE contents of the metasedimentary rocks (157–441 ppm, Kim and Cho, unpublished data). Thus, fractional crystallization is likely to be responsible for the low REE abundance in leucogranite.

The behavior of large ion lithophile elements such as Rb, Sr and Ba is important for deciphering granitoid petrogenesis, because they partition into major rock-forming minerals such as plagioclase, alkali-feldspar and biotite. Trace element compositions of leucogranites (Rb/Ba, 0.2–4.9; Rb/Sr, 1.2–5.3; Sr/Ba, 0.2–1.5) suggest that they are derived from partial melting of metapelitic rocks (Rb/Ba > 0.2; Miller, 1985) through the fluid-absent dehydration melting of biotite (Rb/Sr: 2–6; Sr/Ba: 0.2–0.7; Harris

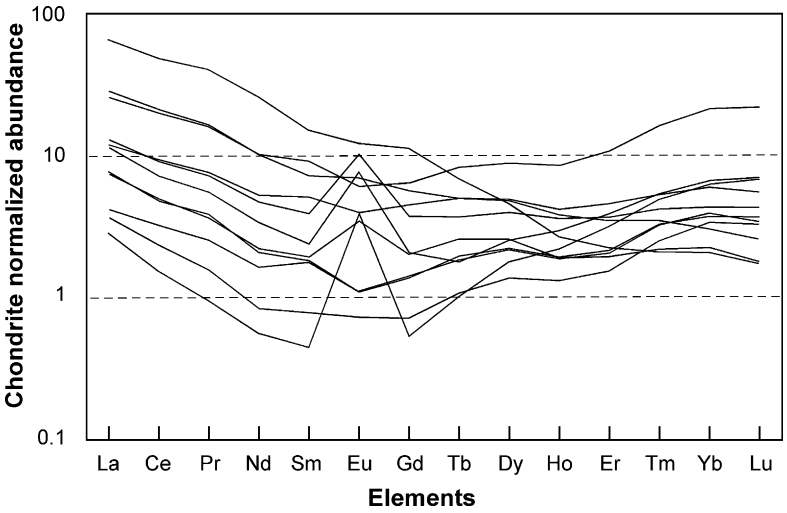

Fig. 6. Chondrite-normalized REE patterns of leucogranite. Normalization values are from Taylor and McLennan (1985).

and Inger, 1992). In addition, the CaO contents (0.4–1.5 wt.%) are compatible with those of pelitic protoliths (CaO < 1.2 wt.%; Miller, 1985). The melt produced by the dehydration melting of muscovite in metapelites has a high K_2O content (>5.5 wt.%), and low FeO_{total} and MgO contents of less than 0.6 and 0.4 wt.%, respectively (McDermott et al., 1996), but these constraints are incompatible with the compositions of leucogranites (Table 1). Thus we conclude that the leucogranites are the product of dehydration melting of biotite. This conclusion is corroborated by the ubiquity of biotite in metasedimentary rocks, in contrast to the rare occurrence of muscovite.

The Rb/Sr and Sr/Ba ratios and the Eu anomaly in granites reflect various mechanisms responsible for the melt formation. Fluid-present melting results in the depletion of K-feldspar in restites and leads to low Rb/Sr and high Sr/Ba ratios in melts, as well as positive Eu anomalies (Harris and Inger, 1992). In contrast, fluid-absent melting causes an increase in restitic feldspars to induce high Rb/Sr and low Sr/Ba together with negative Eu anomalies in the melt. The relationship between the Rb/Sr ratio and the magnitude of the negative Eu anomaly (Fig. 7a) are accounted for by fluid-absent melting of micas (Harris and Inger, 1992). On the other hand, minor variations in Sr/Ba with increasing positive Eu anomaly are not supportive of fluid-present melting to produce the leucogranites.

In order to determine major phases involved in fractional crystallization, Ba and Sr contents of the leucogranites are shown in Fig. 7b, together with the fractionation vectors of plagioclase, K-feldspar and biotite. The Ba and Sr concentrations of the LREE-enriched sample (K47-1) are chosen as the starting melt composition for calculations. Compositional variations in Fig. 7b, together with the lack of biotite in leucogranite, suggest that the major fractionating phase is K-feldspar (Fig. 7b). A few samples with low Sr/Ba exhibit high positive Eu anomalies, indicating that they could represent strongly fractionated feldspathic leucogranites. Fractionation of K-feldspar is also apparent from the positive correlation between the Sr content and the size of the negative Eu anomaly: the former decreases from 152 to 32 ppm, whereas the latter decreases from 3.56 to 0.69.

Tectonic discrimination diagrams using the concentrations of Rb, Y+Nb, and Yb+Ta (Pearce et al., 1984) suggest that the majority of leucogranites plot in the volcanic arc granite (VAG) field, together with a few outliers in the syn-collisional and within plate granite fields (Fig. 8). Similarly, Rb and Y + Nb compositions of the Buncheon granitic gneiss and the Hongjesa granitic batholith in the northeastern Yeongnam Massif (Fig. 1; Hong, 1992) lie mostly in the VAG field, with some falling in the syn-collisional granite

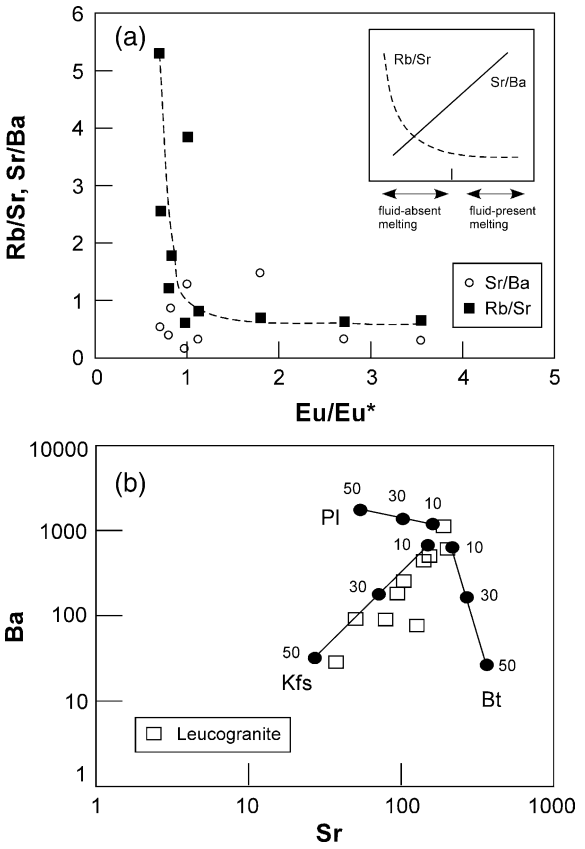

Fig. 7. (a) Variation of Rb/Sr and Sr/Ba vs. the Eu anomaly for leucogranite. The inset figure shows the general trend of Rb/Sr and Sr/Ba in melt for fluid-absent and fluid-present melting. (b) Variation in Ba and Sr concentrations for leucogranite. Mineral vectors are calculated according to partition coefficients of biotite, plagioclase, and K-feldspar from Arth (1976). Closed circles (●) respectively represent 10, 30, and 50% fractionations of each mineral.

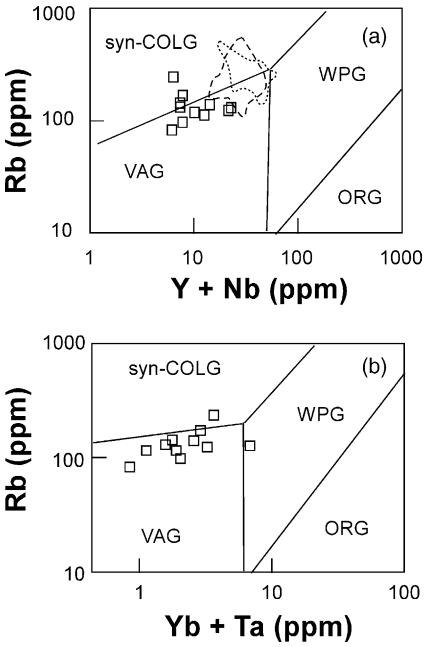

Fig. 8. Tectonic discrimination diagrams based on (a) Rb vs. (Y + Nb); and (b) Rb vs. (Yb + Ta). Open boxes (□) represent the leucogranite compositions. Compositional fields of the Hongjesa granite (dashed field) and Buncheon granitic gneiss (dotted field) are adopted from Hong (1992). Abbreviations: syn-collisional granite (syn-COLG), volcanic arc granite (VAG), within plate granite (WPG) and oceanic ridge granite (ORG).

(Fig. 8a). On the Ta versus Yb discrimination plot (not shown) of Pearce et al. (1984), leucogranites fall in both the VAG and syn-collisional granite fields. Thus, in the absence of tangible evidence for a crustal thickening event, we infer that the leucogranites are formed in an arc-related environment.

6. Isotope geochemistry

The Sm–Nd isotopic data for leucogranite and granitic gneiss are listed in Table 2, and shown in Fig. 9. The Sm–Nd garnet-whole rock age of leucogranite is 1926 ± 41 Ma (mean squares of weighted deviates, MSWD = 79). For granitic gneiss, the garnet-whole rock isochron yields an age of 1928 ± 49 Ma. Although the latter two-point errorchron age is subject to large uncertainty, the Sm–Nd ages for leucogranite and granitic gneiss are indistinguishable from each other. It is thus likely that the Sm–Nd isotope systematics of granitic gneiss has been reset during the emplacement of leucogranite, or that leucogranite generation was synchronous with LP/HT metamorphism.

The Pb–Pb isotopic data are listed in Table 3 and shown in Fig. 10. The granitic gneiss yields an age of 1929 ± 290 Ma (MSWD = 2.8) compatible with the Sm–Nd garnet-whole rock age. On the other hand, leucogranite defines an isochron age of 1862 ± 41 Ma (MSWD = 20), which is consistent with the Sm–Nd age, within error range. In spite of large uncertainties resulting from the limited variations in $^{206}Pb/^{204}Pb$ values, the field relationship supports the view that the

Table 2
Sm–Nd isotopic compositions and model ages of the granitoids and metasedimentary rocks

Sample	Rock type		Sm (ppm)	Nd (ppm)	$^{147}Sm/^{144}Nd$	$^{143}Nd/^{144}Nd$	T_{DM}[a]	ε_{Nd}[b] ($T = 1.9$ Ga)
JJ22-1	Leucogranite	Garnet	0.2126	0.0731	1.7608	0.532064		
		Whole rock	1.682	3.949	0.2577	0.513147		−4.98
YJ13	Leucogranite	Garnet	0.4829	0.7123	0.4101	0.514731		
		Whole rock	0.5376	1.533	0.2122	0.512426		−7.94
YJ21	Leucogranite	Garnet	0.5650	0.4088	0.8360	0.520328		
		Whole rock	2.712	8.729	0.1879	0.512094		−8.51
YP25	Granitic gneiss	Garnet	1.881	7.112	0.1600	0.511888		
		Whole rock	7.502	40.28	0.1127	0.511288	2.65	−5.86
K31	Granitic gneiss	Whole rock	9.108	52.03	0.1059	0.511182	2.63	−6.28
NJ10	Metasediment	Whole rock	11.23	61.71	0.1101	0.511077	2.88	−9.38
YP28-1	Metasediment	Whole rock	10.18	57.07	0.1079	0.511185	2.68	−6.71

[a] Nd model ages following the model of Nägler and Kramers (1998).
[b] ε_{Nd} values were calculated using $^{147}Sm/^{144}Nd = 0.1967$ and $^{143}Nd/^{144}Nd = 0.511847$.

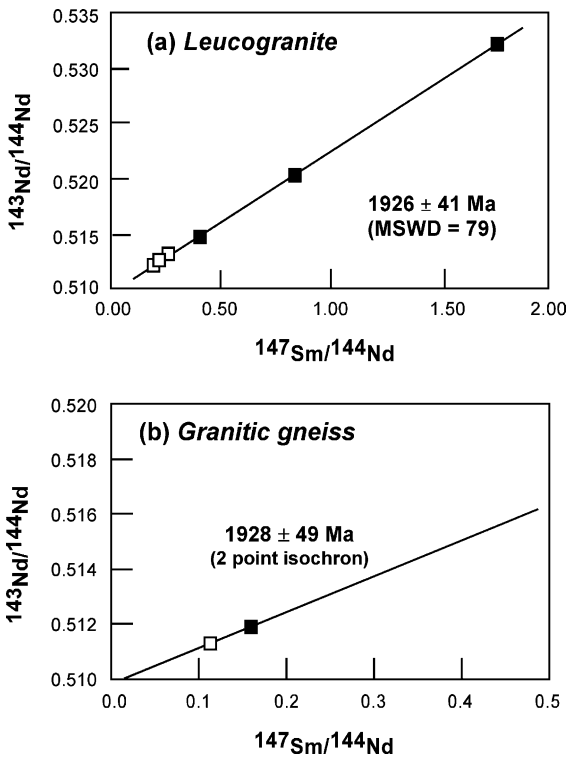

Fig. 9. Sm–Nd isochron diagram for (a) leucogranite and (b) granitic gneiss. Closed (■) and open (□) boxes represent the data points for garnet and whole rock, respectively.

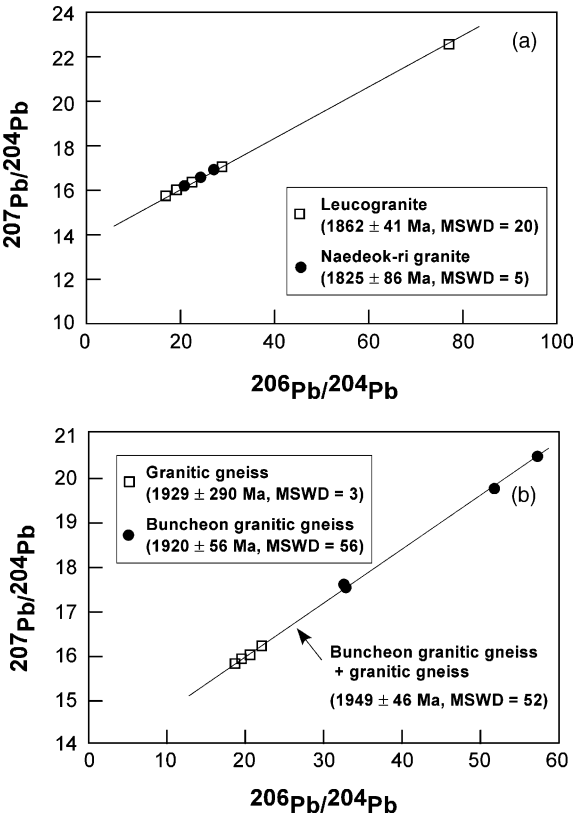

Fig. 10. Pb–Pb whole rock isochron diagram for (a) leucogranite and (b) granitic gneiss. The data for Naedeok-ri granite and Buncheon granitic gneiss are from Park et al. (1993).

Table 3
Pb isotopic compositions of leucogranite and granitic gneiss

	Leucogranite					Granitic gneiss			
	K54	YJ03	YJ13	YJ21	YP28-3	A5-1	A6	K8	YP25
$^{206}Pb/^{204}Pb$	16.896	28.734	22.376	76.982	19.240	19.660	20.645	22.043	18.699
$\pm 2\sigma$	0.084	0.249	0.065	0.144	0.056	0.118	0.112	0.141	0.091
$^{207}Pb/^{204}Pb$	15.727	17.044	16.361	22.592	16.041	15.956	16.057	16.245	15.844
$\pm 2\sigma$	0.087	0.239	0.063	0.143	0.065	0.119	0.102	0.113	0.084
$^{208}Pb/^{204}Pb$	35.903	36.700	35.727	37.245	35.803	40.494	38.814	41.727	40.286
$\pm 2\sigma$	0.094	0.288	0.060	0.157	0.071	0.119	0.101	0.142	0.088

granitic gneiss is the product of an older magmatic event. Major lines of evidence include the field relationship of leucogranite intruding granitic gneiss, and the lack of deformation in leucogranite.

Our Pb–Pb ages of 1862 ± 41 and 1929 ± 290 Ma are also compatible with the whole rock Pb–Pb ages of the Naedeok-ri granite (1825±86 Ma) and the Buncheon granitic gneiss (1920±56 Ma), reported by Park et al. (1993) from the northeastern Yeongnam Massif (Fig. 10; see Figs. 1 and 2 for locations). Buncheon granitic gneiss shows field relationships and deformational fabrics similar to those of the granitic gneiss described here. Pooling of Pb isotopic data of both gneisses yields a combined age of 1949 ± 46 Ma (MSWD = 52). Thus we tentatively suggest that the protolith of the granitic gneisses was emplaced at ca. 1.95 Ga, and subsequently intruded by leucogranite at ca. 1.93–1.86 Ga. Because of large uncertainties involved in the available ages, further studies are necessary to better constrain temporal relationships among granitic rocks.

Granitic gneisses have late Archean T_{DM} model ages (2.65 and 2.63 Ga) with $\varepsilon_{Nd(1.9\,Ga)}$ values of −6.3 and −5.9 (Table 2). The Nd model ages of leucogranites were not estimated because their $^{147}Sm/^{144}Nd$ ratios (0.1879–0.2577) are significantly higher than those of the typical continental crust. This anomaly in leucogranite may be attributed to the fractionation of monazite that is strongly enriched in the LREE (Kröner et al., 2001). Metasedimentary rocks have T_{DM} model ages of 2.88 and 2.68 Ga similar to those of granitic gneisses (Table 2). Thus, both metasedimentary rocks and granitic gneiss represent the product of recycling of late Archean crustal materials. The $\varepsilon_{Nd(1.9\,Ga)}$ values of leucogranite overlap with those of metasedimentary rocks and granitic gneiss. This observation, together with the result from trace element geochemistry, suggests that the parental magma of leucogranite was generated primarily from crustal materials of the Yeongnam Massif with little or minor input from the mantle.

7. Discussion

7.1. LP/HT metamorphism and leucogranite formation

The P–T estimates based on phase equilibria suggest that metasedimentary rocks in the northeastern Yeongnam Massif experienced LP/HT metamorphism and that the peak metamorphic condition in the garnet zone reached ca. 4–6 kbar and 750–800 °C. This result defines a higher metamorphic field gradient than that of normal continental crust, and may require additional heat sources through a combination of magmatic accretion, radioactive heating, aqueous fluid flow, and/or lithospheric extension (e.g., De Yoreo et al., 1991; Gerdes et al., 2000). The coeval Sm–Nd ages of leucogranite and granitic gneiss as well as the field relationship, between leucogranite and migmatitic gneiss, suggest that heat and fluid provided by the leucogranite are pivotal for the LP/HT metamorphism in the metasedimentary rocks. The majority of leucogranites, however, appear to be produced by fluid-absent melting of biotite, as demonstrated by trace element and REE geochemistries. Thus, fluid-absent melting in migmatitic gneisses does not support the view that large-scale fluid flow is a candidate for additional heat source.

Additional sources of heat required for crustal melting and leucogranite formation may be attributed primarily to the underplating of mantle-derived mafic magma or crustal thickening during collisional orogeny. The contribution from shear heating should be minimal because of the lack of large-scale shear zones in the northeastern Yeongnam Massif. Advective heat transport by the underplating of mantle-derived mafic magma is compatible with an arc environment inferred from the trace element geochemistry of leucogranite (Fig. 8). However, evidence for substantial accretion of mafic magma required for significant anatexis in the lower crust (Huppert and Sparks, 1988; Bergantz, 1989) is lacking in the northeastern Yeongnam Massif. Pressure estimates of 4–6 kbar from migmatitic gneisses suggest that the surface exposures of the study area correspond to upper or middle crustal sections. Thus, voluminous occurrence of mafic bodies in the middle to lower crust cannot be ruled out.

An alternative or additional heat source could be attributed to unusually high internal heating from the radiogenic elements (U, Th, and K) in a thick pile of Proterozoic sedimentary rocks (e.g., Gerdes et al., 2000). The present-day concentrations of these elements, estimated from 12 pelitic to psammopelitic schists, are: Th, 19.2 ± 7.0 ppm; U, 4.3 ± 3.3 ppm; and K, 2.9 ± 0.8 wt.% (Kim and Cho, unpublished data). Thus, the radiogenic heat production is estimated as 2.9 ± 1.2 $\mu W\,m^{-3}$ (Philpotts, 1990). This value is higher than ca. 1.8 $\mu W\,m^{-3}$ of the average upper continental crust (calculated from Taylor and McLennan, 1985), and may facilitate crustal melting together with advective heat supplied by underplating.

In summary, the evidence for crustal thickening, e.g., large-scale thrusts or medium- to high-pressure metamorphism, is generally lacking in the northeastern Yeongnam Massif. Thus, the primary heat source for producing parental magma of the leucogranite could be attributed to the underplating of mantle-derived magma in an arc environment. In addition, high abundances of radiogenic elements in metasedimentary rocks suggest at least a partial contribution of radiogenic heating to the thermal budget during leucogranite generation. Further investigations based on isotopic geochemistry and geochronology are needed to confirm the heat source and tectonic setting for leucogranite formation.

7.2. Implications for crustal evolution—correlations between the Yeongnam Massif and Chinese blocks

The available geochronologic and petrologic data, including our own, suggest four stages of crustal growth in the Yeongnam Massif. The earliest crustal formation in the Yeongnam Massif is inferred from the T_{DM} model ages of 2.9–2.5 Ga estimated from metasedimentary rocks and granitic gneisses (Lan et al., 1995; Cheong et al., 2000; Ryoo, 2001; this study). This interpretation is corroborated by the electron microprobe chemical age (ca. 2.7 Ga) of zircon estimated from psammitic gneisses in the southeastern Yeongnam Massif (Ryoo, 2001).

The first widespread magmatism in the Yeongnam Massif is documented at ca. 2.1 Ga as revealed by the Pb–Pb whole rock ages (2160 ± 150 Ma, Kwon et al., 1995; 2093 ± 86 Ma, Cheong et al., 2000) and the U–Pb zircon age (2113 ± 17 Ma, Turek and Kim, 1996) of granitic gneisses. This magmatic event resulted in the formation of the oldest orthogneiss in the Yeongnam Massif. The second magmatic episode at ca. 1.95 Ga has produced the igneous protoliths of granitic gneisses and porphyroblastic gneisses (1920 ± 56 Ma, Pb–Pb whole rock, Park et al., 1993;1945 ± 5 Ma, U–Pb zircon, Turek and Kim, 1996). This magmatic event was followed by the emplacement of the peraluminous leucogranite and Hongjesa granitic batholith at ca. 1.93–1.86 Ga. The last two magmatic episodes are separated by the LP/HT metamorphism and penetrative deformation prevalent in granitic gneisses. The occurrences of undeformed granites with ages of 1825 ± 86 Ma (Pb–Pb whole rock, Park et al., 1993) and high-grade metamorphic rocks with ages of 1840 ± 26 Ma (Pb step-leaching, Cheong et al., 2000) in other parts of the Yeongnam Massif also support the ca. 1.9 Ga magmatic activity broadly coeval with regional metamorphism. This tectonothermal event at ca. 1.9 Ga can be correlated with the Luliangiang Orogeny prominent in the Central Zone, North China Block, which is a product of Paleoproterozoic collision (Wang and Mo, 1995; Zhao, 2001). Diachronous crustal growth and magmatism in the Yeongnam Massif during Paleoproterozoic time are probably common to all Precambrian tectonic blocks in East Asia, and may reflect episodic continental growth culminating at ca.

2.7 and 1.9 Ga to form pre-Rodinian supercontinents (Condie, 2000; Zhao et al., 2002).

Our results have tectonic implications for deciphering the crustal affinity of the Yeongnam Massif with respect to the Gyeonggi Massif and Chinese cratons. The Archean crustal residence ages of ca. 2.9–2.6 Ga in the Gyeonggi Massif (Lee et al., 2000, in press) are consistent with those of the Yeongnam Massif. In addition, the age of prevalent LP/HT metamorphism in the Yeongnam Massif (ca. 1.86 Ga) is compatible with the granulite-facies metamorphism at 1872 ± 7 Ma (ion microprobe U–Pb zircon age) in the northern Gyeonggi Massif associated with collisional tectonics (Lee et al., 2000). The coincidence in the ages of crustal formation and high-temperature metamorphism indicates that both the Yeongnam Massif and Gyeonggi Massif have similar crustal evolution histories until the Paleoproterozoic. However, temporal similarity does not guarantee that both massifs represent a single tectonic unit. It is well known that the North China Block is dominated by Archean crustal growth, whereas the South China Block is characterized by prominent crustal growth during Proterozoic time (Chen and Jahn, 1998). Although Sm–Nd isotopic characteristics and age distributions of both massifs in Korea are similar to those in the North China Block (Lan et al., 1995; Cheong et al., 2000), this consideration could be too simplistic because of recent discoveries of Archean basements in the South China Block (Ma et al., 2000; Qiu et al., 2000) and Mesozoic granites possibly derived from Archean to Early Proterozoic crust (Jahn et al., 2000). Thus, for unraveling the crustal affinity of the Yeongnam Massif, it is probably more useful to consider post-Mesoproterozoic crustal history. However, both the Meso- to Neoproterozoic cover sequences overlying the Paleoproterozoic basement, and the Neoproterozoic tectonothermal events are largely restricted to the Gyeonggi Massif in Korea (e.g., ca. 0.85 Ga, Sm–Nd whole rock isochron, Lee and Cho, 1995; ca. 0.82 Ga, ion microprobe U–Pb age, Cho, 2001). Further studies on post-Mesoproterozoic crustal evolution of the Yeongnam Massif are thus essential for delineating the crustal affinities of the basement terranes in the Korean Peninsula in light of recent developments (e.g., Zhao, 2001) in the Paleoproterozoic crustal evolution of the Chinese cratons.

8. Conclusions

Pelitic to psammopelitic metasedimentary rocks, together with leucogranites and granitic gneisses, are major crustal components in the northeastern Yeongnam Massif. Progressive metamorphic zones, ranging from cordierite through sillimanite to garnet, define low-pressure/high-temperature metamorphism. The peak metamorphic conditions of migmatitic gneisses in the garnet zone reach 750–800 °C and 4–6 kbar. Petrological and geochemical data suggest that fluid-absent melting played a major role in the formation of garnet-bearing leucogranite. The emplacement ages of leucogranite and granitic gneiss are dated at ca. 1.93–1.86 and 1.95 Ga, respectively. These results, together with the available geochronologic data, suggest that Precambrian crustal evolution of the Yeongnam Massif is characterized by the formation of proto-crust at ca. 2.9–2.5 Ga, and several magmatic episodes at ca. 2.1–1.9 Ga. The tectonothermal event at ca. 1.9 Ga, which is possibly correlative with the Luliangiang Orogeny in North China, was accompanied by at least two distinct episodes of felsic magmatism and a low-pressure/high-temperature metamorphic event. Further geochronologic studies are needed to delineate precise relationship between igneous and metamorphic activity that may be associated with or separated by regional deformation, and the tectonic affinity of the Yeongnam Massif.

Acknowledgements

We thank Z.X. Li, S. Wilde and G. Zhao for their helpful and constructive review. We also thank S.R. Lee for providing critical comments on an early version of this paper, and C.-S. Cheong, H. Kim, and B. Chang for their help in isotopic analyses. This study was funded by the Korea Research Foundation Grant (KRF-2000-DA0088) to M. Cho.

References

Aranovich, L.Y., Berman, R.G., 1997. Optimized standard state and solution properties of minerals. II. Comparisons, predictions, and applications. Contrib. Mineral. Petrol. 126, 25–37.

Arth, J.G., 1976. Behavior of trace elements during magmatic processes—a summary of theoretical models and their application. J. Res. U.S. Geol. Surv. 4, 41–47.

Ashworth, J.R., McLellan, E.L., 1985. Textures. In: Ashworth, J.R. (Ed.), Migmatites. Blackie, New York, pp. 180–203.

Bergantz, G.W., 1989. Underplating and partial melting: implications for melt generation and extraction. Science 245, 1093–1094.

Berman, R.G., 1991. Thermobarometry using multi-equilibrium calculations: a new technique, with petrological applications. Can. Mineral. 29, 833–855.

Brown, M., 1983. The petrogenesis of some migmatites from the Presqu'ile de Rhuys, southern Brittany, France. In: Atherton, M.P., Gribble, C.D. (Eds.), Migmatites, Melting and Metamorphism. Shiva, Cambridge, MA, pp. 174–200.

Chen, J., Jahn, B., 1998. Crustal evolution of southeastern China: Nd and Sr isotopic evidence. Tectonophysics 284, 101–133.

Cheong, C.S., Kwon, S.-T., Park, K.-H., 2000. Pb and Nd isotope constraints on Paleoproterozoic crustal evolution of the northern Yeongnam Massif, South Korea. Precam. Res. 102, 207–220.

Cho, M., 2001. A continuation of Chinese ultrahigh-pressure belt in Korea: evidence from ion microprobe U–Pb zircon age. Gondwana Res. 4, 708.

Cho, M., Kwon, S.-T., Ree, J.-H., Nakamura, E., 1995. High-pressure amphibolite of the Imjingang belt in the Yeoncheon-Cheongok area. J. Petrol. Soc. Korea 4, 1–19 (in Korean, with English abstract).

Chough, S.K., Kwon, S.-T., Ree, J.-H., Choi, D.K., 2000. Tectonic and sedimentary evolution of the Korean peninsula: a review and new view. Earth-Sci. Rev. 52, 175–235.

Cluzel, D., 1992. Ordovician bimodal magmatism in the Ogcheon belt (South Korea): intracontinental rift-related volcanic activity. J. Southeast Asia Earth Sci. 7, 195–209.

Condie, K.C., 2000. Episodic continental growth models: afterthoughts and extensions. Tectonophysics 322, 153–162.

De Yoreo, J.J., Lux, D.R., Guidotti, C.V., 1991. Thermal modelling in low-pressure/high-temperature metamorphic belts. Tectonophysics 188, 209–238.

Ebadi, A., Johannes, W., 1991. Beginning of melting and composition of first melts in the system Qz–Ab–Or–H_2O–CO_2. Contrib. Mineral. Petrol. 106, 286–295.

Gerdes, A., Wörner, G., Henk, A., 2000. Post collisional granite generation and HT-LP metamorphism by radiogenic heating: the Variscan South Bohemian Massif. J. Geol. Soc. Lond. 157, 577–587.

Harris, N.B.W., Inger, S., 1992. Trace element modelling of pelite-derived granites. Contrib. Mineral. Petrol. 110, 46–56.

Holtz, F., Pichavant, M., Barbey, P., Johannes, W., 1992. Effects of H_2O on liquidus phase relations in the haplogranitic systems at 2 and 5 kbar. Am. Mineral. 77, 1223–1241.

Holtz, F., Becker, A., Freise, M., Johannes, W., 2001. The water-undersaturated and dry Qz–Ab–Or system revisited. Experimental results at very low water activities and geological implications. Contrib. Mineral. Petrol. 141, 347–357.

Hong, S.S., 2001. Implication for the emplacement depth of the granites in the Yeongnam Massif, using the aluminum-in-hornblende barometry. J. Petrol. Soc. Korea 10, 36–55 (in Korean, with English abstract).

Hong, Y.-K., 1992. Petrogeneses and evolution of early Proterozoic granitic rocks in the northeastern Ryeongnam Massif, Korea. J. Geol. Soc. Korea 28, 571–589.

Huppert, H.E., Sparks, S.J., 1988. The generation of granitic magmas by intrusion of basalt into continental crust. J. Petrol. 29, 599–624.

Inger, S.I., Harris, N.B.W., 1993. Geochemical constraints on leucogranite magmatism in the Langtang Valley, Nepal, Himalaya. J. Petrol. 34, 345–368.

Jacobsen, S.B., Wasserburg, G.J., 1980. Sm–Nd isotopic evolution of chondrites. Earth Planet. Sci. Lett. 50, 139–155.

Jahn, B.-M., Wu, F., Chen, B., 2000. Massive granitoid generation in Central Asia: Nd isotopic evidence and implication for continental growth in the Phanerozoic. Episodes 23, 82–92.

Johannes, W., Holtz, F., 1996. Petrogenesis and Experimental Petrology of Granitic Rocks. Springer, Berlin, p. 335.

KIGAM, 1995. 1:1,000,000 Geologic map of Korea.

Kim, J., Cho, M., 1994. Petrogenesis of the Precambrian Hongjesa granite (magmatism and metamorphism of the Proterozoic in the northeastern part of Korea). J. Petrol. Soc. Korea 3, 76–93.

Kretz, R., 1983. Symbols for rock-forming minerals. Am. Mineral. 68, 277–279.

Kröner, A., Willer, A.P., Hegner, E., Jaekel, P., Nemchin, A., 2001. Single zircon ages, PT evolution and Nd isotopic systematics of high-grade gneisses in southern Malawi and their bearing on the evolution of the Mozambique belt in southeastern Africa. Precam. Res. 109, 257–291.

Kwon, S.-T., Ree, J.-H., Park, K.-H., Jeon, E.-Y., 1995. Nature of contact between the Ogcheon belt and Yeongnam massif and the Pb–Pb age of granitic gneiss in Cheondong-ri, Danyang. J. Petrol. Soc. Korea 4, 144–152 (in Korean, with English abstract).

Lan, C.-Y., Lee, T., Zhou, X.-H., Kwon, S.-T., 1995. Nd isotopic study of Precambrian basement of South Korea: evidence for early Archean crust? Geology 23, 249–252.

Lee, D.S., 1966. Geologic Map of Okdong Quadrangle. National Geological Survey of Korea, p. 30 (in Korean, with English abstract).

Lee, D.W., Kim, S.W., 1965. Geologic Map of Seobyuk-ri Quadrangle. National Geological Survey of Korea, p. 25 (in Korean, with English abstract).

Lee, S.M., Kim, H.S., 1984. Metamorphic studies on the so-called Yulri and Weonnam groups in the Mt. Taebaeg area. J. Geol. Soc. Korea 20, 195–214 (in Korean, with English abstract).

Lee, S.R., Cho, M., 1995. Tectonometamorphic evolution of the Chuncheon amphibolite, central Gyeonggi massif. J. Metam. Geol. 13, 315–328.

Lee, S.R., Cho, M., Yi, K., Stern, R.A., 2000. Early Proterozoic granulites in central Korea: tectonic correlation with Chinese cratons. J. Geol. 108, 729–738.

Lee, S.R., Cho, M., Hwang, J.H., Lee, B., Kim, Y., Kim, J.C., in press. Crustal evolution of the Gyeonggi massif, South Korea: Nd isotopic evidence and implications for continental growths of East Asia. Precamb. Res.

Li, Z.X., 1994. Collision between the North and South China blocks: a crustal-detachment model for suturing in the region east of the Tanlu fault. Geology 22, 739–742.

Li, Z.X., 1998. Tectonic history of the major East Asian lithospheric blocks since the mid-Proterozoic: a synthesis. In: Martin, F.J., Chung, S.-L., Lo, C.-H., Lee, T.-Y. (Eds.), Mantle Dynamics and Plate Interactions in East Asia. AGU, Washington, DC, pp. 221–243.

Ludwig, K.R., 1992. ISOPLOT—a plotting and regression program for radiogenic isotope data, Version 2.75. USGS Open-file Report 91, 445.

Ma, C., Ehlers, C., Xu, C., Li, Z., Yank, K., 2000. The roots of the Dabieshan ultrahigh-pressure metamorphic terrane: constraints from geochemistry and Nd–Sr isotopic systematics. Precam. Res. 102, 279–301.

McDermott, F., Harris, N.B.W., Hawkesworth, C.J., 1996. Geochemical constraints on crustal anatexis: a case study from the Pan-African granitoids of Namibia. Contrib. Mineral. Petrol. 123, 406–423.

Miller, C.F., 1985. Are strongly peraluminous magmas derived from pelitic sedimentary sources? J. Geol. 93, 673–689.

Miyashiro, A., 1961. Evolution of metamorphic belts. J. Petrol. 2, 277–311.

Miyashiro, A., 1994. Metamorphic Petrology. UCL Press, London, p. 404.

Morand, V.J., 1990. Low-pressure regional metamorphism in the Omeo Metamorphic complex, Victoria, Australia. J. Metam. Geol. 8, 1–12.

Nabelek, P.I., Glascock, M.D., 1995. REE-depleted leucogranites, Black Hills, South Dakota: a consequence of disequilibrium melting of monazite-bearing schists. J. Petrol. 36, 1055–1071.

Nägler, T.F., Kramers, J.D., 1998. Nd isotopic evolution of the upper mantle during the Precambrian: models, data and uncertainty of both. Precam. Res. 91, 233–252.

Park, K.H., Cheong, C.S., Lee, K.S., Chang, H.W., 1993. Isotopic composition of lead in Precambrian granitic rocks of the Taebaeg area. J. Geol. Soc. Korea 29, 387–395 (in Korean, with English abstract).

Pattison, D.R.M., 1991. P-T-a(H_2O) conditions in the thermal aureole. In: Voll, G., Töpel, J., Pattison, D.R.M. (Eds.), Equilibrium and Kinetics in Contact Metamorphism. Springer, Heidelberg, pp. 327–350.

Pattison, D.R.M., Harte, B., 1991. Petrography and mineral chemistry of pelites. In: Voll, G., Töpel, J., Pattison, D.R.M. (Eds.), Equilibrium and Kinetics in Contact Metamorphism. Springer, Heidelberg, pp. 135–180.

Pattison, D.R.M., Tracy, R.J., 1991. Phase equilibria and thermobarometry of metapelites. In: Kerrick, D.M. (Ed.), Contact Metamorphism. Reviews in Mineralogy, vol. 26. MSA, pp. 105–206.

Pearce, J.A., Harris, N.B.W., Tindle, A.G., 1984. Trace element discrimination diagrams for the tectonic interpretation of granitic rocks. J. Petrol. 25, 956–983.

Philpotts, A.R., 1990. Principles of Igneous and Metamorphic Petrology. Prentice Hall, London, p. 498.

Qiu, Y.M., Gao, S., McNaughton, N.J., Groves, D.I., Ling, W., 2000. First evidence of >3.2 Ga continental crust in the Yangtze craton of south China and its implications for Archean crustal evolution and Phanerozoic tectonics. Geology 28, 11–14.

Ree, J.-H., Cho, M., Kwon, S.-T., Nakamura, E., 1996. Possible eastward extension of Chinese collision belt in South-Korea: the Imjingang belt. Geology 24, 1071–1074.

Ree, J.-H., Kwon, S.-H., Park, Y., Kwon, S.-T., Park, S.-H., 2001. Pretectonic and posttectonic emplacements of the granitoids in the south central Okchon belt, South Korea: implications for the timing of strike-slip shearing and thrusting. Tectonics 20, 850–867.

Reedman, A.J., Um, S.H., 1975. Geology of Korea. Geol. Min. Inst. Korea, p. 139.

Ryoo, H., 2001. Petrology, geochemistry and geochronology of Precambrian metamorphic rocks in southwestern Yeongnam Massif, South Korea and in North Korea. Unpublished Ph.D. Thesis, Pukyeong University Pusan, Korea, p. 257.

Taylor, S.R., McLennan, S.M., 1985. The Continental Crust: Its Composition and Evolution. Blackwell, Oxford, p. 312.

Turek, A., Kim, C.B., 1996. U–Pb zircon ages for Precambrian rocks in southwestern Ryeongnam and southwestern Gyeonggi Massifs, Korea. Geochem. J. 30, 231–249.

Vernon, R.H., Collins, W.J., 1988. Igneous microstructures in migmatites. Geology 16, 1126–1129.

Wang, H., Mo, X., 1995. An outline of the tectonic evolution of China. Episodes 18, 6–16.

Whittington, A., Harris, N., Baker, J., 1998. Low-pressure crustal anatexis: the significance of spinel and cordierite from metapelitic assemblages at Nanga Parbat, northern Pakistan. In: Treloar, P.J., O'Brien, P.J. (Eds.), What Drives Metamorphism and Metamorphic Reactions? Geol. Soc. London Spec. Pub., pp. 183–198.

Yin, A., Nie, S., 1993. An indentation model for the North and South China collision and the development of the Tan-Lu and Honam fault systems, eastern Asia. Tectonics 12, 801–813.

York, D., 1969. Least squares fitting of a straight line with correlated errors. Earth Planet. Sci. Lett. 5, 320–324.

Zhao, G., 2001. Paleoproterozoic assembly of the North China Craton. Geol. Mag. 138, 89–91.

Zhao, G., Cawood, P.A., Wilde, S.A., Sun, M., 2002. Review of global 2.1–1.8 Ga orogens: implications for a pre-Rodinia supercontinent. Earth-Sci. Rev. 59, 125–162.

Zhao, X., Coe, R.S., Gilder, S.A., Frost, G.M., 1996. Palaeomagnetic constraints on the palaeogeography of China: implications for Gondwanaland. Aust. J. Earth Sci. 43, 643–672.